

UDC 544.526.5

O.L. Stroyuk, S.Ya. Kuchmiy, N.S. Andryushina

SEMICONDUCTOR NANOCRYSTALS AND GRAPHENE OXIDE AS VISIBLE-LIGHT-SENSITIVE PHOTOINITIATORS OF ACRYLAMIDE POLYMERIZATION IN WATER

L.V. Pisarzhevsky Institute of Physical Chemistry of National Academy of Sciences of Ukraine
31 Nauki Pr., Kyiv, 03039, Ukraine, E-mail: stroyuk@inphyschem-nas.kiev.ua

Photopolymerization of acrylamide in aqueous solutions induced by visible light ($\lambda > 400$ nm) absorbed by colloidal particles of $Cd_xZn_{1-x}S$, Fe_2O_3 and graphene oxide is reported. Depending on the photoinitiator nature, primary radicals are generated by monomer reduction with conduction band electrons ($Cd_xZn_{1-x}S$), monomer oxidation by the valence band holes (Fe_2O_3) or by interaction between monomer and free radicals photoeliminated from graphene oxide. The photopolymerization rate increases proportionally to the conduction band potential of $Cd_xZn_{1-x}S$ nanoparticles that depends on their composition. The Fe_2O_3 -initiated acrylamide photopolymerization proceeds with comparable effectiveness in both deaerated and air-exposed aqueous solutions, the feature differing drastically from typical organic photoinitiators. On the basis of kinetic parameters the photopolymerization process was found to be of the chain free radical character with a principal chain termination route being macro-radicals recombination. The kinetic data also indicate a possibility of participation of the $Cd_xZn_{1-x}S$ nanoparticles and graphene oxide in the chain termination.

Keywords: cadmium sulfide, zinc sulfide, iron oxide, graphene oxide, nanocrystals, photocatalysis, photopolymerization

INTRODUCTION

Photoinduced polymerization of unsaturated compounds is of great importance not only for the production of polymer materials but also for the implementation of a number of advanced technologies such as optical information recording, production of printing forms, microelectronic circuit plate, miniature surgical instruments, lenses and prostheses with complex topology and micron (submicron) resolution, removable polymeric templates for lithography and stereolithography, etc. [1–6]. Successful implementation of some of these technologies sometimes put specific demands to the properties of monomers and polymeric products as well as conditions of photopolymerization. For example, photocurable compositions for digital stereolithography should be sensitive to the visible light illuminated by a computer-guided projecting system and produce upon the illumination an easily removable water-soluble polymeric template. The latter requirement can be met by the utilization of monomers, converting upon the illumination into water-soluble polymers, – acrylic and methacrylic acids, acrylamide and its derivatives, vinylpyrrolidone, etc. [5, 6]. At the

same time, choice of an appropriate water-soluble photoinitiator is sometimes problematic for such compositions, since the most widely used water-soluble organic photoinitiators (camphoroquinone, thioxanthone derivatives, titanocenes, dyes, etc.) either absorb only small fraction of the visible light [1–3, 5, 6] or are photochemically unstable.

It was shown that nanometer particles (NPs) of inorganic semiconductors, such as CdS, ZnO, TiO_2 , Fe_2O_3 , etc., could be successfully applied to induce photopolymerization along with traditional organic photoinitiators. Semiconductor NPs manifest quite high efficiency for the initiating of the photopolymerization of various monomers [7–14], they are stable and some of them, for example cadmium sulfide and iron(III) oxide, are sensitive to the visible light. The wide-band-gap semiconductor NPs, such as ZnO and TiO_2 , which have the absorption threshold in the ultraviolet part of the spectrum, can also be used as visible-light-driven photoinitiators provided a dye-sensitizer is added to the photopolymerization composition [12, 14, 15]. At the same time, the majority of reports on the semiconductor NPs-induced photopolymerization are focused on a narrow monomers range, mainly styrene, methylmetha-

crylate and some of its homologues [7, 8, 10–16]. The photopolymerization of water-soluble monomers in the presence of semiconductor NPs remains yet to be studied.

Along with conventional semiconductor materials, the quest for new visible-light-sensitive photoinitiators involves also other new objects, such as, for example, emerging carbonaceous materials including graphene. Recent progress in the chemistry of graphene-based composites is closely related to the studies of chemical transformations of graphene oxide (GO), which can be comparatively easily synthesized via graphite oxidation and ultrasound-assisted exfoliation of the produced graphite oxide [17–20]. In the last years various photochemical and photocatalytic methods of producing new GO-based materials were introduced [21–30], in particular those aimed at the synthesis of heterostructures of partially reduced GO with noble metal [27, 28] and semiconductor NPs [28–30]. At the same time, the photochemistry of GO still remains at a developing stage and many aspects of phototransformations of GO and its photochemical activity are still to be addressed and studied. For example, though recent reports have suggested the free radical character of some stages of the photochemical GO reduction [17, 24], as well as the GO capability of thermal initiation of the polymerization of acryl monomers [31], no mention can be found in the literature about the photochemical activity of GO in free-radical chain reactions, specifically, in the photopolymerization of unsaturated compounds.

In the present work the photopolymerization of acrylamide (AA) in aqueous colloidal solutions of several visible-light-sensitive colloidal species – $\text{Cd}_x\text{Zn}_{1-x}\text{S}$ NPs, Fe_2O_3 NPs and graphene oxide – is reported. The results presented show that semiconductor NPs and colloidal GO can be used as inexpensive, efficient and visible-light-sensitive photoinitiators of the free-radical polymerization of water-soluble acrylic monomers.

MATERIALS AND METHODS

Reagents and synthesis of photoinitiators.

CdCl_2 , ZnCl_2 , FeCl_3 , sodium polyphosphate (SPP), Na_2S , acrylamide (AA), methylviologen (4,4'-dimethylbipyridyl, MV^{2+}) chloride, Na_2SO_3 , KBrO_3 , KBr and KI , graphite powder, KMnO_4 , KClO_3 , HCl and H_2SO_4 were purchased from Sigma Aldrich and used without additional purification. Colloidal $\text{Cd}_x\text{Zn}_{1-x}\text{S}$ NPs

($x = [\text{CdCl}_2]_0 \times \{[\text{CdCl}_2]_0 + [\text{ZnCl}_2]_0\}^{-1}$) were prepared by mixing sodium sulfide with cadmium(II) and zinc(II) chlorides in aqueous SPP solutions. The details of the preparation and characterization of $\text{Cd}_x\text{Zn}_{1-x}\text{S}$ NPs were reported in [32]. Colloidal Fe_2O_3 solutions (1.5×10^{-3} M) were prepared via the prolonged (1–2 h) heating of 3×10^{-3} M FeCl_3 solution at 96–98 °C. Colloidal solutions were kept in the dark at 18–20 °C. Colloidal graphene oxide stabilized by SPP was prepared similarly to [26] by the ultrasonic exfoliation of 50 mg graphite oxide in 100 mL aqueous SPP solution (1×10^{-3} M). Graphite oxide was synthesized by the modified Hummers method via graphite powder oxidation with potassium permanganate in concentrated H_2SO_4 or by the Brodie method via graphite powder oxidation with potassium chlorate in concentrated HCl [17, 18]. The samples of colloidal GO produced from graphite oxide synthesized by the Hummers or Brodie methods are further denoted as H-GO and B-GO, respectively. In a series of experiments prior to the photopolymerization tests the colloidal H-GO was photochemically reduced under the illumination with UV light ($\lambda = 310\text{--}390$ nm) in air with the exposure varying from 30 to 90 min. A detailed study on the properties and photochemical reduction of colloidal SPP-stabilized H-GO is reported elsewhere [26].

Instrumental. Absorption and fluorescence spectra of solutions were registered on a Specord 210 spectrophotometer and a Perkin-Elmer LS55 spectrometer, respectively. The hydrodynamic size (L_{hd}) of colloidal GO particles was measured using a laser photocorrelation spectrometer Malvern Zetasizer Nano. The weight-average molecular mass of polyacrylamide was determined on a liquid-phase chromatograph Du Pont 8800 SLC at 50 °C. XRD diffraction pattern were registered on a DRON-3M diffractometer with the copper K_α line irradiation ($\lambda = 0.1541$ nm). TEM images were obtained using a PEM-125K apparatus with an accelerating voltage of 100 kV.

The acrylamide photopolymerization was studied in glass 10.0-mm optical cuvettes at room temperature. Prior to illumination the sample solutions (2.5 mL) were bubbled with the argon flow during 10–15 min to remove dissolved oxygen, and then the cuvettes were sealed. The solutions were illuminated by the focused light from a high-pressure 1000 W mercury lamp using various combinations of the standard optical glass

filters to adjust the spectral range to $\lambda = 310\text{--}390$ nm, $\lambda > 420$ nm or $\lambda > 460$ nm. To avoid heating of the sample solutions in the course of illumination, a 50.0 mm glass cuvette filled with water was placed between the light source and the work cuvette. The light intensity was varied by using calibrated metal grids.

Monomer concentration determination. In case of semiconductor NPs the monomer concentration was measured by double bond bromination followed by iodometric determination of residual bromine. In a typical procedure, 0.2 mL aliquot of a tested solution was added to 8.0 mL of a solution containing 0.50 M H_2SO_4 and 0.11 M KBr followed by the 0.8 mL 0.05 M KBrO_3 solution. The mixture was kept in dark at room temperature for 10–15 min to complete the bromination. Then 1.0 mL 2.0 M potassium iodide solution was added to the mixture. In 5 min 0.1 mL aliquot was taken from the mixture and introduced into 9.9 mL KI 2.0 M solution. The optical density of the resulting KI_3 solutions at 351 nm was measured and used for the calculation of the monomer concentration.

Colloidal graphene oxide interferes with the bromination method and therefore, in GO-based photopolymerization systems a viscosity of solution was taken as a parameter proportional to the reaction rate. The viscosity of illuminated solutions was measured using a vibration viscometer Malvern SV-100 with a certainty of $\sim 1\%$.

RESULTS AND DISCUSSION

Characterization of photoinitiators.

1.1 Colloidal CdS and $\text{Cd}_x\text{Zn}_{1-x}\text{S}$ NPs. Reaction between a mixture of cadmium and zinc chlorides and sodium sulfide in aqueous SPP solutions results in formation of stable colloidal $\text{Cd}_x\text{Zn}_{1-x}\text{S}$ solutions provided the precursor concentrations not exceed 1×10^{-2} M. At small concentrations, $(1\text{--}5) \times 10^{-4}$ M, the Cd:Zn ratio in $\text{Cd}_x\text{Zn}_{1-x}\text{S}$ NPs deviates somewhat from that in the initial solution [32] due to faster precipitation of CdS as compared to ZnS and partial binding of Zn^{II} in complexes with OH^- , water and other species. In this connection, more concentrated sols (5×10^{-3} – 1×10^{-2} M) were used in the present work, where Cd:Zn ratio was the same in both the starting Cd^{II} and Zn^{II} chloride solution and the colloidal $\text{Cd}_x\text{Zn}_{1-x}\text{S}$ NPs. Fig. 1a represents diffraction patterns of the coagulates collected from the solutions with $[\text{Cd}_x\text{Zn}_{1-x}\text{S}] = [\text{SPP}] = 5 \times 10^{-3}$ M. The diffraction patterns reveal three broadened peaks indicating the presence of NPs with a cubic zinc blende crystalline motive. The size of $\text{Cd}_x\text{Zn}_{1-x}\text{S}$ NPs calculated using the Scherer formula was found to be around 3 nm independently of the NPs composition. Interplanar distances in $\text{Cd}_x\text{Zn}_{1-x}\text{S}$ NPs change with x according to the Vegard law (Fig. 1b) so indicating $\text{Cd}_x\text{Zn}_{1-x}\text{S}$ NPs to be homogeneous solid solutions.

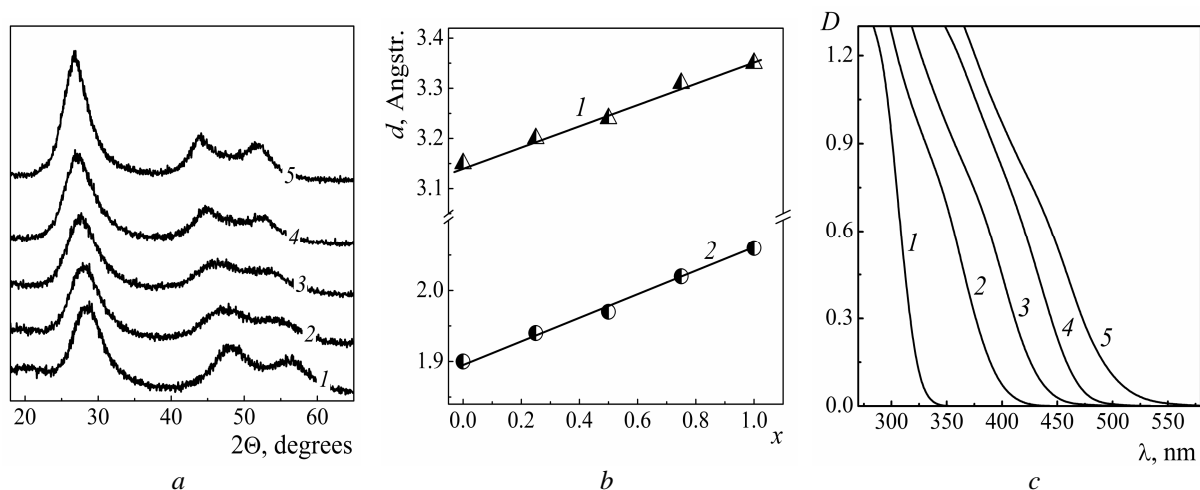


Fig. 1. (a) X-Ray diffraction patterns of $\text{Cd}_x\text{Zn}_{1-x}\text{S}$ NPs at $x = 0$ (curve 1), 0.25 (2), 0.50 (3), 0.75 (4) and 1.00 (5); (b) interplanar distance d_{111} (curve 1) and d_{220} (2) as a function of x ; (c) absorption spectra of SPP-stabilized colloidal $\text{Cd}_x\text{Zn}_{1-x}\text{S}$ solutions at $x = 0$ (curve 1), 0.25 (2), 0.50 (3), 0.75 (4), 1.00 (5). $[\text{Cd}_x\text{Zn}_{1-x}\text{S}]_0 = [\text{SPP}] = 5 \times 10^{-3}$ M, cuvette – 2.0 mm

Position of the absorption threshold (λ_{tr}) of colloidal SPP-stabilized $Cd_xZn_{1-x}S$ NPs was found to depend on x and on the concentration of both reagents and stabilizer. At $[Cd_xZn_{1-x}S] = [SPP] = 5 \times 10^{-3}$ M, a variation of x from 0 to 1.0 results in the λ_{tr} shift from 330–335 nm (Fig. 1 c, curve 1) to 510–515 nm (Fig. 1 c, curve 5) corresponding to a decrease of the band gap E_g from 3.75 to 2.5 eV.

1.2 Colloidal Fe_2O_3 NPs. Boiling of aqueous iron(III) chloride solutions results in the salt hydrolysis and formation of stable brownish-red iron(III) oxide colloids. Electron diffraction (ED) pattern of freshly prepared colloidal Fe_2O_3 particles

(Fig. 2 a) reveals only two weak circles and a central halo indicating the most part of iron oxide particles to be amorphous. Ageing of the colloidal solutions is accompanied by continuous crystallization of Fe_2O_3 particles as evident from an increase in the number of the circles in ED patterns and the circle narrowing. The ED pattern of Fe_2O_3 particles after 20 days ageing consists of at least seven distinct reflexes (Fig. 2 b) corresponding to the interplanar distances of 1.54, 1.88, 2.16, 2.52, 3.04, 3.61 and 4.18 Å typical for hematite α - Fe_2O_3 [33–36].

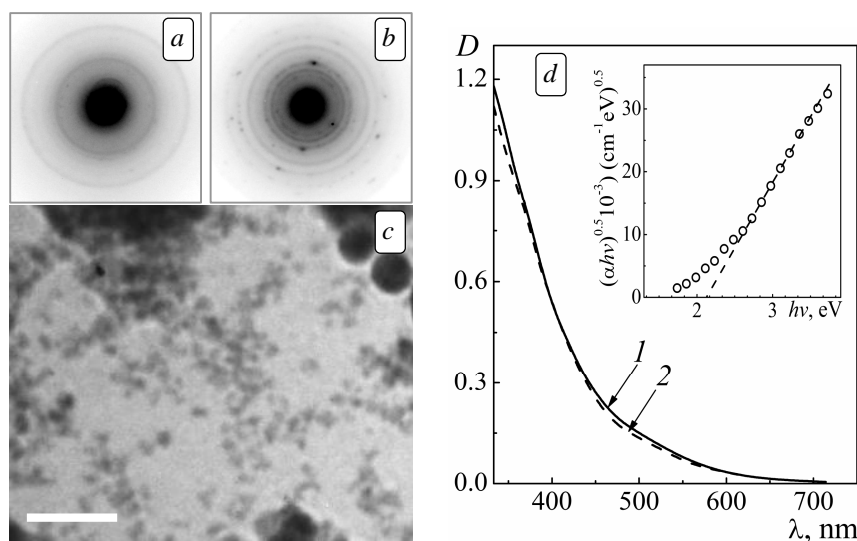


Fig. 2. Electron diffraction patterns (negative images) of freshly prepared (a) and aged for 20 days (b) colloidal Fe_2O_3 solution; (c) TEM image of Fe_2O_3 nanoparticles aged for 20 days (scale bar is 50 nm); (d) absorption spectra of freshly prepared (curve 1) and aged for 20 days (2) Fe_2O_3 colloid. $[Fe_2O_3] = 5 \times 10^{-4}$ M, cuvette – 10.0 mm. *Insert in (d):* curve 2 in the coordinates “ $(\alpha hv)^{0.5} - hv$ ”

TEM image of the iron oxide particles aged for 20 days is presented in Fig. 2 c. Two major NP fractions can be observed – small 4–6 nm and larger 20–30 nm particles. Despite the differences in the crystallinity, the absorption spectra of both freshly prepared and aged colloidal Fe_2O_3 solutions are almost identical and consist of a featureless absorption band smoothly descending throughout the visible spectrum range (Fig. 2 d). A section of the spectral curves with $hv > 2.5$ eV was found to be linear in the coordinates “ $(\alpha hv)^{0.5} - hv$ ”, where $\alpha(hv) = 2303\rho D(hv)CM^{-1}l^{-1}$ (ρ is the density of hematite, 5.24 g/cm³, $D(hv)$ is the optical density of the solution, corresponding to the quantum energy hv , C is the colloidal solution concentration in g/cm³, M is the molar mass of iron(III) oxide and l

is the optical path). It can be therefore concluded that the observed absorption band originates from an indirect interband electron transition in hematite NPs [37, 38]. Extrapolation of the linear spectrum anamorphosis to the zero ordinate (insert in Fig. 1 d) gives the band gap of Fe_2O_3 particles $E_g = 2.12 \pm 0.02$, the value being in accordance with the well-known E_g of the bulk hematite (2.0–2.2 eV [38–41]). Light absorbance at $hv < E_g$ is supposed to originate from defect states in the band gap near to the conduction (valence) band edge [37, 38].

1.3 Colloidal graphene oxide. Colloidal SPP-stabilized GO solutions were prepared by ultrasound-assisted exfoliation of graphite oxide in aqueous SPP solutions as described in [26]. The method allows us to prepare colloidal GO with the

concentration of up to 500 mg/L retaining stability toward aggregation during the year and longer. An atomic force microscopy study of GO particles showed them to be 1.2–1.4-nm thick with a lateral size of GO sheets varying from 150–200 nm to several microns (Fig. 3 *a, b*). A dynamic light scattering study of SPP-stabilized GO colloids showed that the average hydrodynamic size (L_{hd}) of colloidal GO sheets was around 320 nm indicating

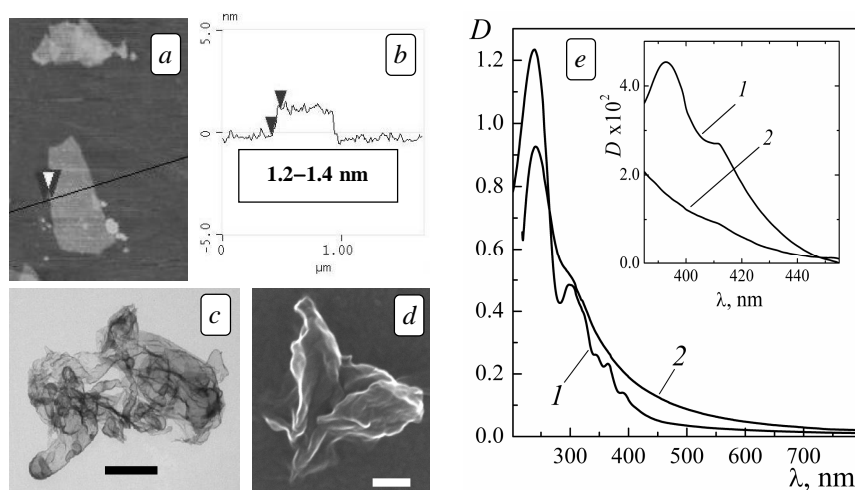


Fig. 3. (a) AFM image of graphene oxide particles; (b) roughness profile of a H-GO particle for a section marked by a line in (a); (c, d) TEM (c) and SEM (d) image of a single folded and crumpled H-GO particle; scale bar is 500 (c) and 200 nm (d); (e) absorbance spectra of colloidal B-GO (curve 1) and H-GO (2). Insert shows enlarged sections of the absorbance spectra after subtraction of the background absorbance of the sp^2 -hybridized carbon fragments of the GO particles

Oxidation "depth" of the colloidal GO determines its optical properties (Fig. 3 *e*), in particular, the position of a characteristic maximum at $\lambda_g = 220$ – 240 nm, the intensity of $n\pi$ -bands of the functional groups in the range of 290–400 nm, and intensity of a longer-wavelength absorption band at $\lambda > 400$ nm originating from electron transitions in the non-oxidized aromatic domains of sp^2 -hybridized carbon in graphene oxide sheets [17, 18].

Reduction of GO is typically accompanied by a "red" shift of λ_g toward the position typical for graphene and graphite (~ 270 nm), extinction of the $n\pi$ -bands and an increase of the light absorbance in the visible and near IR spectral ranges. For graphene oxide samples produced by the Brodie and Hummers methods, the characteristic λ_g maximum resides at 238 and 240 nm, respectively (Fig. 3 *e*). As shown in [26], the photoreduction of colloidal SPP-stabilized H-GO by UV light ($\lambda = 310$ – 390 nm) results in a shift of λ_g to 257–258 nm, almost complete elimination of the

that they were crumpled and partially folded in solution, this observation also being in accordance with those by using transmission electron (Fig. 3 *c*) and scanning electron (Fig. 3 *d*) microscopy. The results of infrared and NMR ^{13}C spectroscopy discussed in [26] showed that both H-GO and B-GO sheets were decorated predominantly by epoxy-, $-OH$, $-C=O$, and $-COOH$ groups.

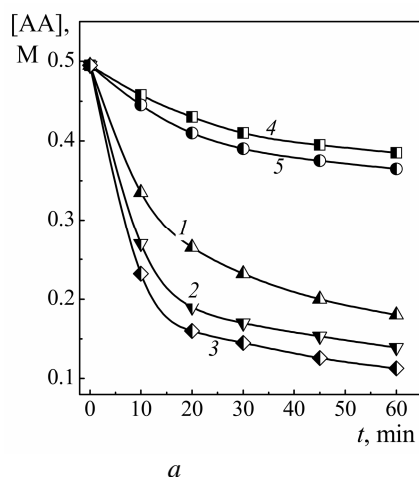
$n\pi$ -band and an increase in the absorbance of the sp^2 -carbon domains of GO particles in the visible and near IR parts of the spectrum.

The B-GO sample exhibits a combination of several $n\pi$ -bands at $\lambda = 290$ – 400 nm, obviously belonging to different oxygen-containing functionalities (Fig. 3 *e*, curve 1). The insert in Fig. 3 *e* shows fragments of the spectra of colloidal B-GO and H-GO after subtraction of the continuous background introduced by the light absorption by sp^2 -domains. It is evident that in the range of $\lambda > 400$ nm corresponding to the photoexcitation of the polymerization systems under study, the integral $n\pi$ -band intensity of the B-GO sample is almost twice as large as that for the H-GO sample, indicating a much higher content of the oxygen-containing functional groups in the B-GO.

General characterization of acrylamide photopolymerization. 2.1 Colloidal CdS and $Cd_xZn_{1-x}S$ NPs as photoinitiators. Complete and equivalent light absorption by $Cd_xZn_{1-x}S$ NPs throughout the entire range of x values can be

achieved only if the solutions are illuminated by a short-wave source, for example, with a mercury 253.9 nm line. However, under such illumination non-catalytic spontaneous photopolymerization of acrylamide was found to take place. So, to avoid possible interference of non-catalytic and photocatalytic processes, a longer-wave mercury lines with $\lambda = 313$ and 365 nm was used to excite $\text{Cd}_x\text{Zn}_{1-x}\text{S}$ NPs and therefore the NP range restricted to $x \geq 0.3$.

When there is no photocatalyst present in a monomer solution (0.5–10.0 M), the AA concentration remains constant at prolonged (3–4 h) illumination. In the presence of CdS or $\text{Cd}_x\text{Zn}_{1-x}\text{S}$ NPs, fast reduction of the monomer concentration and growth of the solution viscosity due to polymer formation are observed. The facts indicate that the photocatalytic polymerization takes place with the participation of semiconductor NPs. Fig. 4 *a* shows



kinetic curves of the AA photopolymerization in solutions of various compositions. A comparison of the curves 1 and 2 in Fig. 4 *a* shows that about half the monomer is converted into the polyacrylamide in the initial 10–15 min of the illumination with 70–80 % monomer conversion after 1 h illumination. A gradual slowing of the photopolymerization can be accounted for by the monomer consumption and NP surface blocking by the polymer.

Both the conduction band electrons and the valence band holes can initiate the photopolymerization *via* respectively reduction or oxidation of a monomer to ion-radicals. At the same time, the valence band potentials of both CdS and $\text{Cd}_x\text{Zn}_{1-x}\text{S}$ NPs are sufficiently high for the monomers oxidation ($E_{\text{VB}} \geq 1.6$ V versus standard hydrogen electrode, SHE).

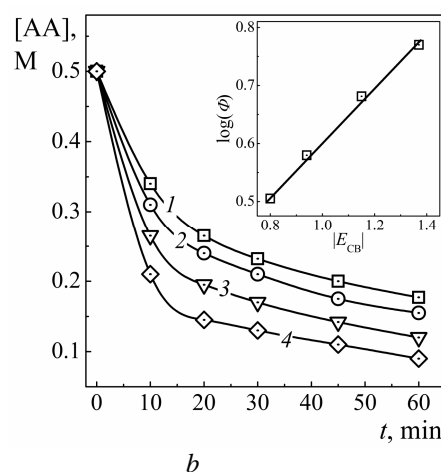


Fig. 4. (a) Kinetic curves of acrylamide photopolymerization in degassed solutions in the presence of CdS (curve 1) and $\text{Cd}_{0.5}\text{Zn}_{0.5}\text{S}$ NPs (2) only, CdS NPs and Na_2SO_3 (3), CdS NPs and MV^{2+} (4), and $\text{Cd}_{0.5}\text{Zn}_{0.5}\text{S}$ NPs and MV^{2+} (5); (b) Kinetic curves of acrylamide photopolymerization in degassed solutions induced by CdS (curve 1), $\text{Cd}_{0.75}\text{Zn}_{0.25}\text{S}$ (2), $\text{Cd}_{0.5}\text{Zn}_{0.5}\text{S}$ (3) and $\text{Cd}_{0.3}\text{Zn}_{0.7}\text{S}$ NPs (4). *Insert:* A semilogarithmic relationship between the quantum yield of AA photopolymerization and the conduction band potential of $\text{Cd}_x\text{Zn}_{1-x}\text{S}$ NPs. $[\text{Cd}_x\text{Zn}_{1-x}\text{S}] = 1 \times 10^{-3}$ M, $[\text{SPP}] = 3 \times 10^{-3}$ M, $[\text{AA}] = 0.5$ M, $[\text{Na}_2\text{SO}_3] = 0.1$ M, $[\text{MV}^{2+}] = 1 \times 10^{-3}$ M

A relative contribution of the conduction band electrons and valence band holes into the photoinitiation of the polymerization can be estimated separately by the help of agents capable of selective scavenging of one sort of the charge carriers. In such a way, a relative contribution of e_{CB}^- can be deduced studying the photopolymerization in the presence of sodium sulfite, which can scavenge h_{VB}^+ and suppress the monomers oxidation. On the other hand, carrying out the photopolymerization in the presence of MV^{2+} one

can eliminate a contribution of monomer reduction by e_{CB}^- . A comparison of the curves 1 and 4 or 2 and 5 in Fig. 4 *a* shows that the photopolymerization rate falls by a factor of four – from 2.75×10^{-4} to 0.7×10^{-4} M/s in the case of CdS NPs and from 3.83×10^{-4} to 0.92×10^{-4} M/s in the case of $\text{Cd}_{0.5}\text{Zn}_{0.5}\text{S}$ NPs, when the photoreaction is carried out in the presence of methylviologen. It should be noted that the photopolymerization rate does not fall to zero, although the MV^{2+} concentration is three orders higher than that sufficient for complete

scavenging of the photogenerated electrons. The fact speaks in favor of the h^+_{VB} participation in the photopolymerization, the relative contribution of this channel of primary radical generation not exceeding 25 %. The conclusion about the dominating role of e^-_{CB} in the photoinitiation is also supported by a 60 % increase in the photopolymerization rate, from 2.75×10^{-4} to 4.47×10^{-4} M/s (compare curves 1 and 3 in Fig. 4 a) when Na_2SO_3 is introduced. Sulfite ions, though suppressing complementary photoinitiation route with the participation of h^+_{VB} , impede strongly the recombination processes and so promote the monomer reduction by e^-_{CB} .

The rate of AA photopolymerization in air-exposed solutions is only by a third smaller than that observed in degassed solutions. It can therefore be concluded that oxygen does not affect noticeably the primary photochemical events on the surface of semiconductor NPs. This is a striking feature of the semiconductor NPs distinguishing them from organic photoinitiators. The absence of any induction period during the first 5–10 min of the photopolymerization in the presence of air indicates that oxygen is a weak inhibitor in the systems under investigation. It is known that during an initial stage of the radical photopolymerization oxygen can build into the growing polymer chain giving regular $-(\text{M-O-O-M-O-O})_n-$ structures (where M is a monomer) [42–44]. There is approximately 3×10^{-4} M of the oxygen in air-saturated water at 18–20 °C [45]. Taking into account that typical photopolymerization rates are $(2.0\text{--}5.0) \times 10^{-4}$ M/s, one can expect a sharp decrease in O_2 concentration in the first minutes of the photoreaction, while the diffusion of new portions of oxygen would be hindered due to increased viscosity of a solution and lack of the stirring.

It is widely accepted that the photopolymerization of acrylic monomers in aqueous solutions proceeds only *via* a free-radical mechanism [42, 44]. This mechanism implies transformation of primary charged monomer ion-radicals into neutral radical species. As probable routes for these transformations the protonation of an anion-radical and the deprotonation of a cation-radical deprotonation can be assumed [44]. The CdS and $\text{Cd}_x\text{Zn}_{1-x}\text{S}$ NPs act as an efficient photocatalyst of hydrogen evolution from aqueous solutions [46, 47]. In this view, an alternative scheme of primary radicals generation can be proposed

assuming primary neutral radical generation *via* hydrogen atom addition to a monomer molecule. To assess the probability of this photoinitiation route, an effect of AA on the photocatalytic hydrogen evolution from an aqueous solution of sodium sulfite (1×10^{-2} M) and $\text{Cd}_{0.5}\text{Zn}_{0.5}\text{S}$ NPs (5×10^{-3} M) was studied. This process becomes noticeably slower already in the presence of small amounts of AA ($\sim 10^{-3}$ M) and is quenched completely at $[\text{AA}] = 1 \times 10^{-2}$ M, confirming feasibility of atomic hydrogen participation in the generation of primary monomer radicals.

Fig. 4 b shows kinetic curves of the AA photopolymerization in the presence of $\text{Cd}_x\text{Zn}_{1-x}\text{S}$ NPs of various compositions. The variation of the quantum yield of the photoprocess with x (Table 1) also supports the assumption about the dominating role of monomer reduction with e^-_{CB} in formation of primary radicals. It can be seen from Table 1 that the quantum yield grows from 3.2 to 5.8 with the molar Cd(II) fraction in $\text{Cd}_x\text{Zn}_{1-x}\text{S}$ NPs decreasing from 1.0 to 0.3. Experimental conditions being the same, one can deduce that an increase in the quantum yield from CdS to $\text{Cd}_{0.75}\text{Zn}_{0.25}\text{S}$ to $\text{Cd}_{0.5}\text{Zn}_{0.5}\text{S}$ to $\text{Cd}_{0.3}\text{Zn}_{0.7}\text{S}$ originates from an increase in the primary radical formation rate.

The valence band potential E_{VB} of the bulk cadmium and zinc sulfides is 1.6 V [48, 49] and 1.8 V [46, 50] versus NHE respectively. Combining these values with the band gap energies E_g of bulk cubic CdS (2.4 eV) [48, 49] and ZnS (3.6 eV) [46, 50], we obtain the conduction band potentials for cadmium sulfide $E_{CB} = -0.8$ V and zinc sulfide $E_{CB} = -1.8$ V. Comparison of both E_{CB} values shows that the conduction band increment from CdS to ZnS (1.0 eV) is 5 times higher than that of the valence band potential (0.2 V). The dependence between the quantum yield of AA photopolymerization and the composition of $\text{Cd}_x\text{Zn}_{1-x}\text{S}$ NPs is therefore likely to originate not from the variation of the valence band energy but from the E_{CB} increase with decreasing x .

A difference between the E_{VB} values of cadmium and zinc sulfides being comparatively small, using a simple linear combination (1) for the calculation of $E_{VB}(x)$ would not apparently introduce substantial error into the determination of the E_{CB} of $\text{Cd}_x\text{Zn}_{1-x}\text{S}$ NPs from eq. (2):

$$E_{VB}(x) = xE_{VB}(\text{CdS}) + (1-x)E_{VB}(\text{ZnS}), \quad (1)$$

$$E_{CB}(x) = E_{VB}(x) - E_g(x). \quad (2)$$

The E_{CB} values computed by this method for CdS and $Cd_xZn_{1-x}S$ NPs at $x = 0.3, 0.5$ and 0.75 are presented in Table 1. It can be seen from the table that Φ increases along with the augmentation of the conduction band potential of the semiconductor NPs.

Table 1. Quantum yield Φ of AA photopolymerization in the presence of $Cd_xZn_{1-x}S$ NPs with a different conduction band potential E_{CB}

	x	Φ	E_{CB}, V
1	0.30	5.8	-1.37
2	0.50	4.8	-1.15
3	0.75	3.8	-0.94
4	1.00	3.2	-0.80

Notes: Φ was determined at $[Cd_xZn_{1-x}S] = 1 \times 10^{-3} M$, $[SPP] = 3 \times 10^{-3} M$, $[AA] = 0.5 M$

Correlations between a rate constant of the interfacial charge transfer k_{et} (which determines the quantum yields of the photoinitiation and the photopolymerization as a whole) and the energies of an electron donor E_D ($E_D = E_{CB}(x)$ in the case under discussion) and an acceptor E_A (here – one-electron acrylamide reduction potential E_{AA}) can be described by the Tafel equation [50, 51]:

$$\log(k_{et}/k_{et}^0) = \alpha(E_D - E_A) \quad (3)$$

where k_{et}^0 is a charge transfer rate constant at a standard potential, α is a coefficient. If the observed $\Phi - x$ dependence is actually determined by the overvoltage of AA reduction by e^-_{CB} , $E_{CB}(x) - E_{AA}$, a linear dependence between $\log(\Phi)$ and $E_{CB}(x)$ should exist. This was found to be the case (see insert in Fig. 4 b), supporting an assumption about the crucial role of the rate of electron transfer from the conduction band of $Cd_xZn_{1-x}S$ NPs to monomer molecules.

2.2 Colloidal Fe_2O_3 NPs as a photoinitiator.

Illumination of the solutions where both AA and Fe_2O_3 NPs are present, with the UV ($\lambda = 310-390$ nm) or visible light ($\lambda = 400-600$ nm), results in a gradual decrease of the monomer concentration and growth of the solution viscosity due to polymer formation. In the absence of iron oxide NPs, AA concentration remains constant at prolonged illumination (3–4 h). It can be concluded that Fe_2O_3 NPs act as the photoinitiator of AA polymerization. There holds a balance between the mass of the monomer consumed to the moment when the photoreaction is stopped and the mass of a polymeric product, the fact indicating the

photopolymerization be the sole path of monomer consumption.

If the photoinitiation of AA polymerization involves conduction band electrons, similarly to $Cd_xZn_{1-x}S$ NPs, a fall of the photopolymerization rate after the admission of air into the reaction mixture can be expected, since the oxygen is an efficient electron acceptor. It was found though, that the photopolymerization rate decreases only slightly (~10–15 %), when oxygen molecules are present in a solution. So, one can conclude that e^-_{CB} does not reduce neither oxygen nor the monomer, the valence band holes being apparently the basic participant of primary radicals generation. The same conclusion can be derived from the evaluation of the energetic characteristics of the photopolymerization system components. The E_{VB} of hematite is +1.85 V versus SHE at pH 14 [53]. The most part of the presented experiments were performed in neutral solutions with the initial monomer concentration $[AA]_0 = 0.5 M$. At pH 7 $E_{VB}(\alpha-Fe_2O_3) = +2.26 V$ (SHE). So, the conduction band potential of the colloidal iron(III) oxide NPs with $E_g = 2.12 eV$ is also positive, $E_{CB} = +0.14 V$ (SHE). This potential is apparently too low for one-electron reduction of oxygen ($E^0 = -0.33 V$, SHE [53]). Though the exact value of the AA reduction potential is not to be found in literature, it is known that the reduction potentials of acrylic acid derivatives are in general close to -1 V (SHE) [8, 54]. Hence, the direct AA reduction by the Fe_2O_3 NPs conduction band electrons is also unfavorable.

The indirect monomer radicals generation via the AA reduction by the hydrogen atoms, which can form at the water reduction by e^-_{CB} can also be discarded because $E(H^+/H^\bullet) = -0.41 V$ (SHE) at pH 7. Additional experiments showed that no molecular hydrogen forms even at a trace amount at prolonged illumination of iron(III) oxide colloids. Summarizing, one can conclude that the most probable way of the primary radicals generation in the system under investigation is the AA oxidation by the Fe_2O_3 valence band holes.

The molecular mass of polyacrylamide (PAA) produced in air-saturated solutions, $(0.7 \pm 0.1) \times 10^6$ g/mol, is substantially lower than that of the polymer obtained from degassed solutions, $(1.2 \pm 0.1) \times 10^6$ g/mol. This can be due to the participation of oxygen in the chain termination reactions [Fe30, Fe31].

It has been found that photocatalytic activity of Fe_2O_3 NPs in the photoinitiation of AA polymerization depends notably upon the duration of the colloidal solution ageing (Fig. 5). Upon the ageing of Fe_2O_3 NPs during 1–10 days, a constant growth of the rate of AA photopolymerization is observed, the stationary photoactivity being achieved in 12–20 days. Taking into consideration the above-discussed TEM and ED results, the growth of photocatalytic activity of Fe_2O_3 NPs upon ageing can be associated with gradual crystallization of the colloidal semiconductor and a decrease in the fraction of amorphous iron(III) oxide. It is a well-known fact that oxide semiconductors, for example, TiO_2 , manifest noticeable photocatalytic activity only when being in the crystalline state [55–57]. Very fast recombination processes in amorphous semiconductors [58] result evidently in the suppression of the photochemical reactions.

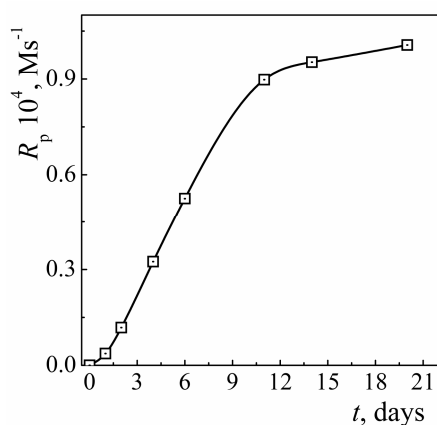


Fig. 5. Relationship between the ageing duration of colloidal Fe_2O_3 solution and the rate of acrylamide photopolymerization in the presence of air. $[\text{Fe}_2\text{O}_3] = 3 \times 10^{-4} \text{ M}$, $[\text{AA}]_0 = 0.5 \text{ M}$, $I = 1.67 \times 10^{-7} \text{ Einstein/s}$

2.3 Colloidal graphene oxide as a photoinitiator. Illumination of argon-saturated solutions containing both the SPP-stabilized GO and acrylamide by the visible light ($\lambda > 400 \text{ nm}$) results in an increase in the solution viscosity proportional to the exposure (Fig. 6). In the absence of the monomer the viscosity remains constant under illumination and by the value close to the viscosity of both water and the monomer solution kept in the dark for the same time period (Table 2, rows 1 and 2).

These observations suggest that GO acts as a visible-light-sensitive photoinitiator of the AA polymerization. The weight-average molecular mass of the polyacrylamide produced was found to be $\sim 1 \times 10^5 \text{ g/mole}$ (at 0.8 M AA and 0.1 mg/mL H-GO).

Illumination of the AA-containing solutions saturated with air does not result in any changes in the viscosity so evidencing that the molecular oxygen acts as an efficient inhibitor of the photoinduced polymerization in the system under discussion. In this view GO behaves as a typical organic molecular photoinitiator. The average molecular mass and molecular mass distribution of the polyacrylamide were found to be constant in the first 60–90 min of the photopolymerization, so the solution viscosity can be assumed to be directly proportional to the polymer molecules number. As the photoinduced viscosity changes in the time range studied is of almost linear character (Fig. 6), an increment of the solution viscosity at a given illumination period, for example, the first 30 min, can be used as a measure of the photopolymerization rate.

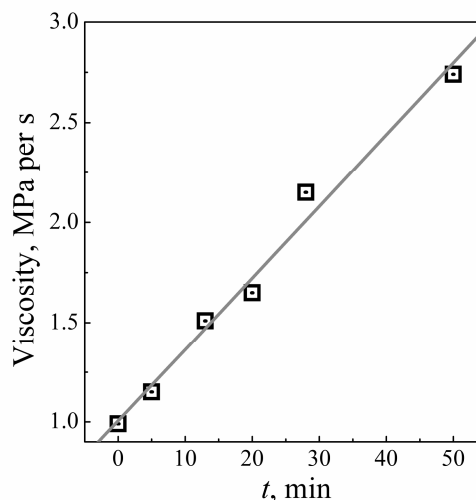


Fig. 6. Change of the viscosity of the colloidal GO solution (0.1 mg/mL) illuminated by the visible light in the presence of 0.8 M acrylamide. $[\text{SPP}] = 1 \times 10^{-3} \text{ M}$

These observations suggest that GO acts as a visible-light-sensitive photoinitiator of the AA polymerization. The weight-average molecular mass of the polyacrylamide produced was found to be $\sim 1 \times 10^5 \text{ g/mole}$ (at 0.8 M AA and 0.1 mg/mL H-GO). Illumination of the AA-containing solutions saturated with air does not result in any changes in the viscosity so evidencing that the molecular oxygen acts as an efficient inhibitor of the photoinduced polymerization in the system under discussion. In this view GO behaves as a typical organic molecular photoinitiator. The average molecular mass and molecular mass distribution of the polyacrylamide were found to

be constant in the first 60–90 min of the photopolymerization, so the solution viscosity can be assumed to be directly proportional to the polymer molecules number. As the photoinduced viscosity changes in the time range studied is of

almost linear character (Fig. 6), an increment of the solution viscosity at a given illumination period, for example, the first 30 min, can be used as a measure of the photopolymerization rate.

Table 2. Viscosity of deaerated aqueous solutions of acrylamide kept under various conditions

N	Conditions	Viscosity, mPa·s
1	kept in the dark for 30 min in the presence of H-GO	1.01
2	illuminated...	1.07
3	...without additives	4.62
4	...in the presence of B-GO	2.68
5	...in the presence of H-GO	1.82
6	illuminated in the presence of H-GO, which was preliminary photoreduced by	1.57
7	excitation at $\lambda = 310\text{--}390$ nm for...	1.06
8	illuminated in the presence of H-GO at $\lambda > 460$ nm	1.05

Notes: $[AA]_0 = 0.8$ M, $[GO] = 0.1$ mg/mL, the wavelength range of illumination in 1–7 – $\lambda > 400$ nm, exposure – 30 min. The viscosity of distilled water at 25 °C is 0.89 mPa·s

The efficiency of AA photopolymerization was found to depend critically on the oxidation degree of colloidal GO. In particular, the most efficient photoinitiator is B-GO, that is the graphene oxide synthesized by the Brodie method (Table 2, line 3), which carries the largest amount of the oxygen-containing functional groups [17, 18]. Although the integral $n\pi$ -band intensity of the B-GO sample is almost twice as large as that for the H-GO sample indicating a much higher content of the oxygen-containing functional groups in the B-GO, the photopolymerization rate is almost two times higher for B-GO than for the less oxidized H-GO (Table 2).

Photochemical reduction of H-GO under the illumination in the range of $\lambda = 310\text{--}390$ nm [26] prior to the photopolymerization experiments results in further deterioration of the capability of graphene oxide to induce photopolymerization of acrylamide (lines 4–6) till the almost complete loss of photoactivity for the photoreduced H-GO produced at 90 min illumination (Table 2, line 7). In the latter case the chromatographic measurements confirmed absence of any polymeric species in solutions after 60–90 min illumination with the visible light ($\lambda > 400$ nm). Moreover, at illumination of H-GO – AA solutions with the longer-wavelength light, $\lambda > 460$ nm, that is out of the absorbance range of the $n\pi$ -bands of graphene oxide, no increment of the solution viscosity was observed as well (Table 2, line 8). So, two basic factors determining GO activity in AA photopolymerization are (i) the content of the oxygen-

containing functionalities contributing to the $n\pi$ absorption band and (ii) correspondence between the spectral range of excitation light and the range of $n\pi$ -absorbance of graphene oxide.

Taking into consideration the capability of GO to photochemical transformations [21–26], one may expect that at the photoinduced polymerization of acrylamide, concurrent photoreduction of GO should also occur. At the same time, experimental data indicate that the latter process either does not take place or occurs with negligible efficiency. In particular, illumination of the “B-GO – AA” systems at $\lambda > 400$ nm during 40–50 min results in a mere 15–20 % lowering of the integral intensity of the $n\pi$ -bands with their number and shape unchanged, while complete extinction of the $n\pi$ -band is usually observed at exciting B-GO in the spectral range of 310–390 nm. Besides, separate experiments showed that the photoreduction of B-GO alone by the UV light resulted in almost complete quenching of the B-GO fluorescence already in the first minutes of exposure. At the same time, only minor changes of the B-GO fluorescence band parameters were detected when the “B-GO – AA” system was excited at $\lambda > 400$ nm during the entire course of the photochemical experiment, so indicating very low rate of the B-GO photoreduction in such conditions. Finally, as shown here, preliminary photoreduction of H-GO results in deterioration of its capability of photoinitiating of acrylamide polymerization. At the same time, the

photopolymerization rate was found to be almost independent on the light exposure (Fig. 6). Therefore, we can neglect possible photoreduction of graphene oxide when analyzing the kinetic features of the GO-induced acrylamide photopolymerization.

Kinetic aspects of acrylamide photopolymerization. 3.1 Influence of monomer concentration. $Cd_{0.5}Zn_{0.5}S$ and Fe_2O_3 NPs. Fig. 7

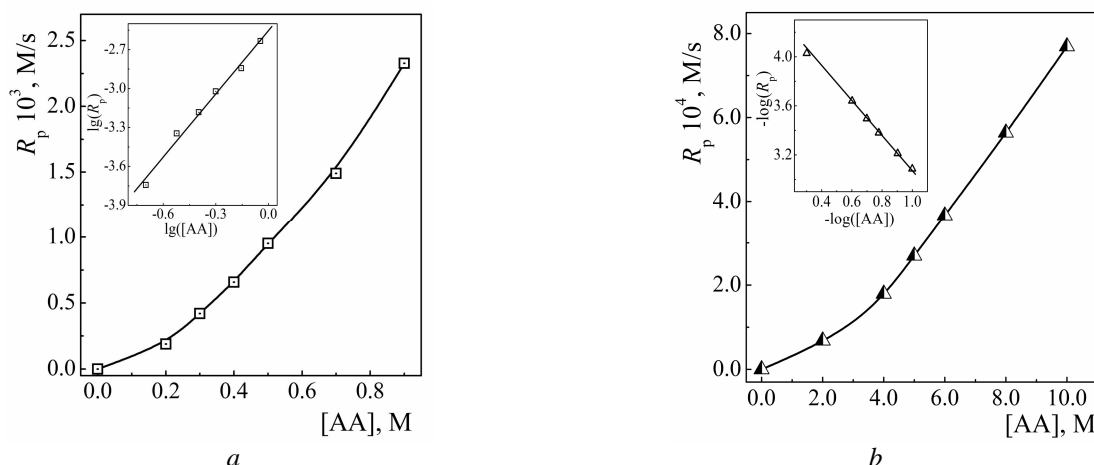


Fig. 7. Rate of AA photopolymerization in the presence of $Cd_{0.5}Zn_{0.5}S$ (a) and Fe_2O_3 NPs (b) versus the initial monomer concentration. *Inserts:* the same dependences in logarithmic coordinates. $[Cd_{0.5}Zn_{0.5}S] = 1 \times 10^{-3}$ M, $[SPP] = 3 \times 10^{-3}$ M, $[Fe_2O_3] = 3 \times 10^{-4}$ M (aged for 20 days), $I = 1.67 \times 10^{-7}$ Einstein/s

A linear dependence between the rate and the initial monomer concentration is usually observed ($n_M = 1.0$) when the chain-radical photopolymerization of acrylic monomers is initiated by molecular photoinitiators [42, 44]. As the most probable reason for the kinetic reaction order by the monomer higher than unity, the participation of the monomer in primary radicals generation can be assumed. Indeed, when molecular photoinitiators (for example carbonyl aromatic compounds, polyvalent metal complexes [3, 44], dyes [44, 45, 59], etc.) are used to induce photopolymerization, the light absorption results either in photoinitiator decomposition or its transition into an excited state, which interacts further with components of a solution, in particular, with a solvent, giving primary radicals. At that the monomer reacts either with primary radicals generated from a photoinitiator or with growing polymer chain, participating exclusively in the chain propagation stage. In the systems under discussion a monomer oxidation by h^+_{VB} or its reduction by e^-_{CB} results directly in the monomer radicals formation. Involvement of the monomer

illustrates a dependence between the AA photopolymerization rate and the starting AA concentration for $Cd_{0.5}Zn_{0.5}S$ (a) and Fe_2O_3 NPs (b). Kinetic orders by the monomer concentration, $n_M = 1.45 \pm 0.05$ ($Cd_{0.5}Zn_{0.5}S$) and $n_M = 1.5 \pm 0.1$ (Fe_2O_3) were calculated from the logarithmic transforms of the curves presented in Fig. 7 (see inserts).

into both the photoinitiation and chain propagation results in an increase of n_M up to 1.5. Not only the photopolymerization rate but also the molecular mass of polymeric products depend upon the initial monomer concentration. In air-saturated solutions of $Cd_{0.5}Zn_{0.5}S$ NPs (1×10^{-3} M) and AA the molecular mass of polyacrylamide is 0.2×10^6 at $[AA]_0 = 0.5$ M, $(0.45-0.50) \times 10^6$ at $[AA]_0 = 0.75$ M, and $(1.25-1.30) \times 10^6$ at $[AA]_0 = 1.0$ M.

Graphene oxide. The AA photopolymerization rate was found to grow at increasing the monomer concentration reaching a "plateau" in the range of $[AA] > 0.8$ M and then remaining almost unchanged at further increase in the AA concentration (Fig. 8a). A dynamic light scattering study on colloidal "GO – AA" systems showed that introduction of acrylamide and further elevation of its concentration result in a drastic increase of the hydrodynamic radius L_{hd} of H-GO particles (Fig. 8b) as a result of their aggregation. In the absence of acrylamide a peak of L_{hd} distribution is located at 120–140 nm (curve 1). As 0.5 M monomer is introduced into the solution the average L_{hd} shifts

to 200–250 nm, the distribution broadens and a highly aggregated fraction of GO appears with the average L_{hd} value at 2.5–3.0 μm (curve 2). Further increase in the AA concentration to 1.0 M results in almost complete aggregation of GO particles (curve 3).

As established by the chromatography, the molecular mass of the polyacrylamide produced at $[\text{AA}] = 0.6 \text{ M}$ and $[\text{AA}] = 1.2 \text{ M}$ is the same. Therefore, the plateau on the dependence given in Fig. 8a reflects slowing of the photoinitiation with

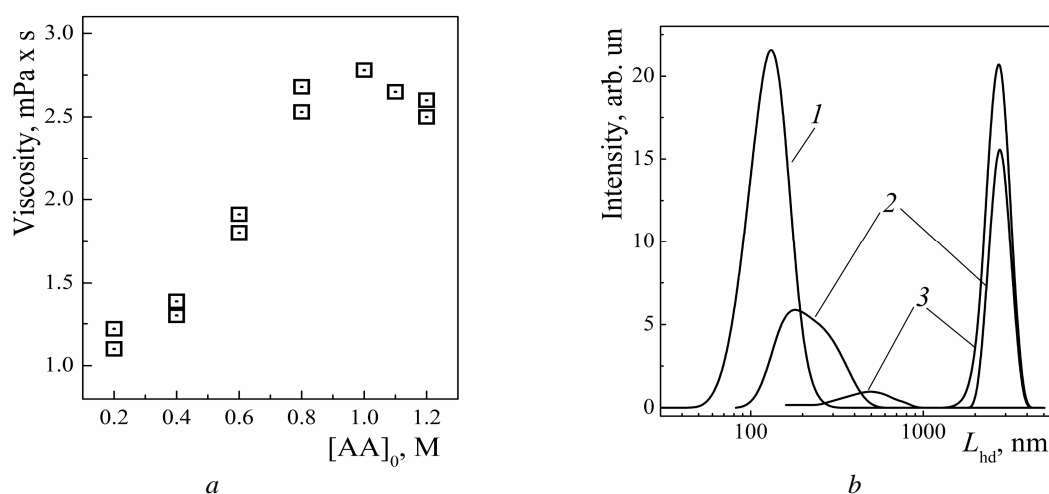


Fig. 8. (a) Viscosity of the photopolymerization systems after 30-min exposure at different starting concentration of acrylamide; $[\text{H-GO}] = 0.1 \text{ mg/mL}$, $[\text{SPP}] = 1 \times 10^{-3} \text{ M}$; (b) distribution of colloidal H-GO particles by the hydrodynamic radius (L_{hd}) without monomer (curve 1) and with 0.5 M (2) and 1.0 M acrylamide (3). $[\text{H-GO}] = 0.025 \text{ mg/mL}$, $[\text{SPP}] = 1 \times 10^{-3} \text{ M}$

The kinetic reaction order by the monomer concentration derived from a section of the dependence, corresponding to $[\text{AA}] < 1.0 \text{ M}$, was found to be $n_M = 0.9 \pm 0.1$, that is close to the value $n_M = 1.0$ expected for the “classic” case of free-radical photopolymerization when a monomer does not participate immediately in the photochemical generation of primary radicals. Again, in this view GO resembles classical organic photoinitiators rather than the semiconductor NPs. In the “graphene oxide – AA” system primary radicals are most probably generated via photoinduced elimination of functional groups from the basal plane of GO sheets. The GO photoreduction with the light quanta larger than $\sim 3 \text{ eV}$ ($\lambda < 415 \text{ nm}$) is assumed to proceed via elimination of carbonyl and carboxyl groups in the form of CO and CO₂ molecules producing the radicals H^\bullet (OH^\bullet) and R^\bullet (R is the bulk of a GO particle) recombining immediately [24]. It is reported also that graphene

oxide is capable of thermal initiation of the free-radical polymerization of N-vinylpyrrolidone [31]. As detected by EPR in [31], the radical centers were produced even at mild heating of GO suspensions.

Initiation of the photopolymerization can also involve –OH groups of GO. Photoinduced migration of these functionalities to the periphery of sp^2 -carbon domains in the basal plane of GO is currently assumed to be one of the basic mechanisms of expansion of the aromatic system of conjugated sp^2 -carbon atoms at the GO photoreduction [17, 18]. A couple of radical centers generated by breaking the C–OH bonds apparently can induce the polymerization of acrylamide. Alternatively, the primary radicals can also be supplied from water oxidation by the photoexcited GO [26].

3.2 Influence of light intensity. $\text{Cd}_x\text{Zn}_{1-x}\text{S}$ and Fe_2O_3 NPs. Relationships between the light

intensity I and the AA photopolymerization rate in the presence of $\text{Cd}_x\text{Zn}_{1-x}\text{S}$ NPs (Fig. 9 *a*, curve 1), Fe_2O_3 NPs (curve 2) and graphene oxide (Fig. 9 *b*)

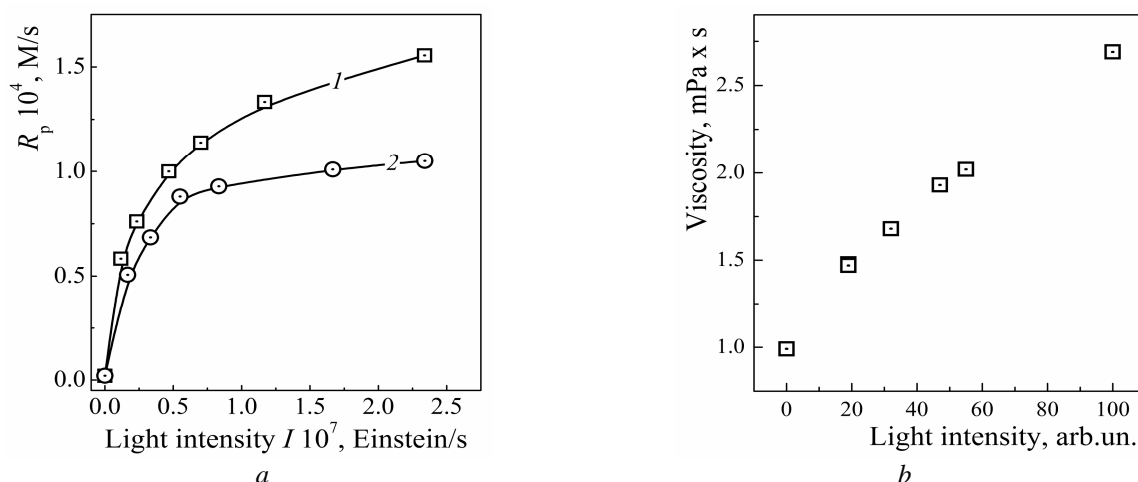


Fig. 9. The rate of acrylamide photopolymerization versus light intensity I for $\text{Cd}_{0.5}\text{Zn}_{0.5}\text{S}$ NPs (*a*, curve 1) and Fe_2O_3 NPs (*a*, curve 2); $[\text{AA}] = 0.5 \text{ M}$, $[\text{Cd}_{0.5}\text{Zn}_{0.5}\text{S}] = 1 \times 10^{-3} \text{ M}$, $[\text{SPP}] = 3 \times 10^{-3} \text{ M}$, $[\text{Fe}_2\text{O}_3] = 3 \times 10^{-4} \text{ M}$ (aged for 20 days); (*b*) viscosity of the photopolymerization system based on graphene oxide after 30-min exposure at a different relative intensity of the light flux; $[\text{AA}] = 0.8 \text{ M}$, $[\text{SPP}] = 1 \times 10^{-3} \text{ M}$. In (*b*) $[\text{H-GO}] = 0.1 \text{ mg/mL}$

The kinetic polymerization orders by the light intensity are $n_1 = 0.33 \pm 0.02$ for $\text{Cd}_x\text{Zn}_{1-x}\text{S}$ NPs, $n_1 = 0.38 \pm 0.07$ for Fe_2O_3 NPs, and $n_1 = 0.40 \pm 0.05$ for H-GO. A somewhat lower than expected value of n_1 is often observed when the relaxation of electron excitation of a photoinitiator depends in a non-linear manner upon the excitation light intensity I . For example, n_1 is usually not higher than 0.3–0.4 for the photopolymerization induced by semiconductor NPs [7–14], when the primary photochemical reactions compete with electron-hole recombination, the rate of the latter being proportional to I^2 [60]. In graphene oxide the energy supplied by the photoexcitation of oxygen-containing chromophores can be transferred to aromatic sp^2 -clusters and then be consumed for activation of chemical processes (for example migration of $-\text{OH}$ group). The aromatic sp^2 -carbon domains surrounded by the sp^3 -carbon matrix of GO can be considered as a “flat” analogue of the semiconductor NP embedded into a dielectric material, that is the radiative electron-hole recombination in sp^2 -carbon domains can also depend in a non-linear manner on the excitation light intensity. Deviation of n_1 from the expected value can be associated with the recombination processes in sp^2 -carbon domains of GO competing with the primary photochemical processes.

are described by a power dependence typical for the free-radical photopolymerization of acrylic monomers [43, 44].

3.3 Influence of photoinitiator concentration.
CdS and $\text{Cd}_x\text{Zn}_{1-x}\text{S}$ NPs. A correlation between the initial rate of the acrylamide photopolymerization and the molar $\text{Cd}_{0.5}\text{Zn}_{0.5}\text{S}$ concentration is given in Fig. 10 *a* for both degassed (curve 1) and aerated (curve 2) solutions. The plateau on the curve 1 at $[\text{Cd}_{0.5}\text{Zn}_{0.5}\text{S}] > 8 \times 10^{-4} \text{ M}$ can originate from saturation of the light absorbance. A difference in the form of the curves 1 and 2 is probably due to the fact that at low NPs contents, when the light absorption and consequent primary radicals concentration is low, O_2 consumption is slow allowing effective quenching of the macro-chains growth.

Iron oxide NPs. The photocatalytic AA polymerization in the presence of air is of considerable interest first of all from the practical viewpoints, for example, for the photochemical PAA synthesis or for the design of photocurable compositions [61, 62]. So, the kinetics of the photocatalytic polymerization was studied mostly in air-exposed systems. Fig. 10 *b* illustrates a dependence of the photopolymerization rate upon the molar Fe_2O_3 concentration. It is of an S-like shape originating most probably from the efficient inhibition by oxygen at low photocatalyst content. When the Fe_2O_3 concentration is elevated, the light absorbance of the photopolymerization system and the primary radicals concentration grow too,

making the inhibitive oxygen effect less pronounced. It was found that at low photoinitiator concentrations ($[\text{Fe}_2\text{O}_3] = 5 \times 10^{-5} \text{ M}$) evacuation of the reaction mixtures resulted in an almost ten-fold R_p increase. At $[\text{Fe}_2\text{O}_3] > 3 \times 10^{-4} \text{ M}$ saturation of the light absorption is achieved and the further growth of the iron oxide concentration does not affect considerably the photopolymerization rate. When the complete light absorbance is achieved,

the photopolymerization rate remains virtually constant in a wide range of the NP concentration (Fig. 10 *b*). One can therefore conclude that semiconductor NPs do not participate in the termination of growing polymer chains. This conclusion is supported also by the fact that the molecular mass of polyacrylamide does not noticeably change at the variation in the iron oxide concentration from 3×10^{-4} to $1.5 \times 10^{-3} \text{ M}$.

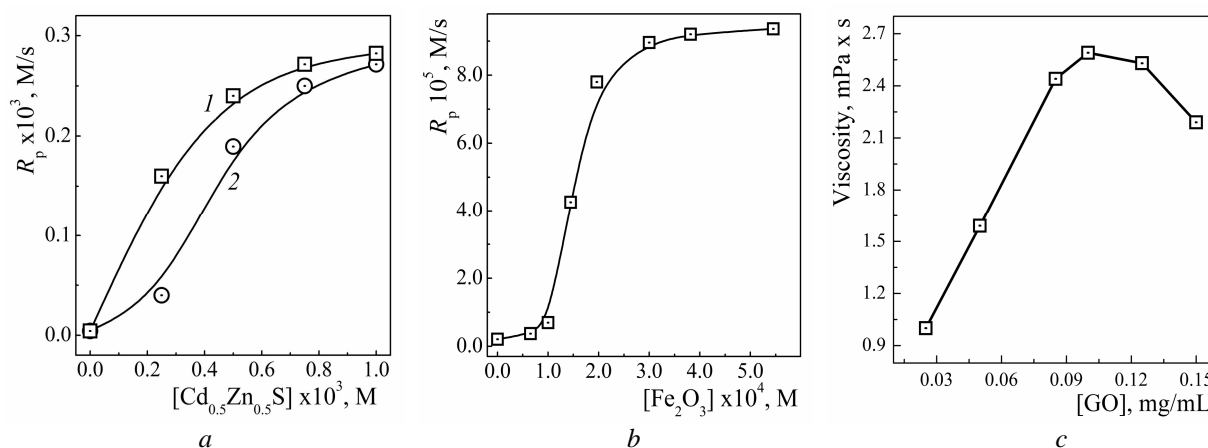


Fig. 10. (*a, b*) Rate of acrylamide photopolymerization induced by $\text{Cd}_{0.5}\text{Zn}_{0.5}\text{S}$ NPs (*a*) in degassed (curve 1) and air-saturated (2) solutions and by Fe_2O_3 NPs in air-saturated solution (*b*) versus molar semiconductor concentration; $[\text{AA}] = 0.5 \text{ M}$, $I = 1.67 \times 10^{-7} \text{ Einstein/s}$; (*c*) viscosity of H-GO-based photopolymerization system after 30-min exposure at a different concentration of H-GO; $[\text{AA}] = 0.8 \text{ M}$, $[\text{SPP}] = 1 \times 10^{-3} \text{ M}$. In (*c*) $[\text{H-GO}] = 0.1 \text{ mg/mL}$

Graphene oxide. The final viscosity of the photopolymerization systems was found to grow with an increase in H-GO concentration reaching a maximal value at $[\text{GO}]$ around 0.1 mg/mL and decreasing at a higher GO content (Fig. 10 *c*). According to the dynamic light scattering data, an increase in GO concentration in the range studied does not result in any appreciable changes of the hydrodynamic size of colloidal GO particles. A decrease in the photopolymerization rate at $[\text{GO}] > 0.1 \text{ mg/mL}$ cannot, therefore, be associated with the aggregation of GO particles as was assumed above when interpreting the correlation between the photopolymerization rate and the monomer concentration. No decrease was observed in the viscosity of the photopolymerization composition at $[\text{GO}] > 0.1 \text{ mg/mL}$ be associated with the light filtration by the photoinitiator because even at the highest GO concentration the optical density of work solutions at $\lambda > 400 \text{ nm}$ did not exceed 1.0. Taking these observations into account, the most probable origin of the extreme nature of the dependence given in Fig. 10 *c* is

participation of the GO particles in termination of the growing macro-radicals. In accordance with this assumption the weight-averaged molecular mass of polyacrylamide produced on the right side of the maximum, at $[\text{GO}] = 1.5 \text{ mg/mL}$ was found to be by 40–50 % lower than that of the polymer produced on the left side of the maximum, at $[\text{GO}] = 0.05 \text{ mg/mL}$. The capability of GO to interact with growing polymer chains is well known and has recently been used to graft GO with polyacrylamide, polyacrylic acid [63], and polyvinyl acetate [64].

CONCLUSIONS

The photopolymerization of acrylamide induced by visible light ($\lambda > 400 \text{ nm}$) absorbed by colloidal particles of $\text{Cd}_x\text{Zn}_{1-x}\text{S}$ ($x > 0.3$), hematite Fe_2O_3 and graphene oxide is reported. In the case of $\text{Cd}_x\text{Zn}_{1-x}\text{S}$ NPs the dominant pathway of the generation of primary radicals was suggested to be the reduction of adsorbed monomers by the conduction band electrons of $\text{Cd}_x\text{Zn}_{1-x}\text{S}$ nanoparticles. Two complimentary photoinitiation

channels were assumed to exist – the monomer oxidation by the valence band holes and the addition of photocatalytically produced hydrogen to monomer molecules. For Fe_2O_3 NPs with the conduction band potential lower than the redox-potential of monomer, water or oxygen reduction, the principal route of primary radical generation is oxidation of the monomer by the photogenerated valence band holes. In graphene oxide-based system the photoinitiation was found to proceed with the participation of oxygen-containing fragments of graphene oxide particles, the photopolymerization rate growing with an increase in the content of such functional groups and *vice versa* lowering drastically at their photoinduced elimination.

A correlation between the composition of $\text{Cd}_x\text{Zn}_{1-x}\text{S}$ NPs and their photocatalytic activity in the polymerization of acrylamide was found. Growth of the conduction band potential of the semiconductor nanoparticles at an increase in the molar Zn^{II} fraction was suggested as the main

reason for the growth of the quantum efficiency of the photocatalytic polymerization.

The Fe_2O_3 NPs-initiated acrylamide photopolymerization proceeds with comparable effectiveness in both deaerated and air-exposed aqueous solutions at comparatively low photoinitiator concentrations ($[\text{Fe}_2\text{O}_3] < 1 \times 10^{-3} \text{ M}$) and yields polyacrylamide with relatively high molecular mass ($1.2 \times 10^6 \text{ g/mol}$ in degassed solutions and $0.7 \times 10^6 \text{ g/mol}$ in the air-containing systems).

On the basis of the kinetic analysis of the photopolymerization process it has been found that the photoinitiation is achieved most probably at the interaction between acrylamide and primary free radicals produced by photoexcitation of semiconductor NPs or graphene oxide while the basic chain termination route is recombination of the growing macro-radicals. The kinetic data also indicate possibility of $\text{Cd}_x\text{Zn}_{1-x}\text{S}$ NPs and graphene oxide participation in the chain termination.

Нанокристали напівпровідників та оксид графену – чутливі до видимого світла фотоініціатори полімеризації акриламід у воді

О.Л. Стрюк, С.Я. Кучмій, Н.С. Андрюшина

*Інститут фізичної хімії ім. Л.В. Писаржевського Національної академії наук України
пр. Науки, 31, Київ, 03039, Україна, stroyuk@inphyschem-nas.kiev.ua*

Досліджено фотополімеризацію акриламід у водних розчинах, індуковану при дії видимого світла ($\lambda > 400 \text{ нм}$) на колоїдні частинки $\text{Cd}_x\text{Zn}_{1-x}\text{S}$, Fe_2O_3 та оксиду графену. В залежності від природи фотоініціатора, первинні радикали утворюються при відновленні мономера фотогенерованими електронами зони провідності (у випадку $\text{Cd}_x\text{Zn}_{1-x}\text{S}$), окисненні мономера фотогенерованими дірками валентної зони (Fe_2O_3) або ж внаслідок взаємодії між мономером та вільними радикалами, що утворюються в результаті фотолізу ініціатора (оксид графену). Швидкість фотополімеризації зростає пропорційно абсолютному значенню потенціалу зони провідності наночастинок $\text{Cd}_x\text{Zn}_{1-x}\text{S}$, який визначається їх складом. Фотополімеризація акриламід, індукована наночастинами Fe_2O_3 , відбувається однаково ефективно як в дегазованих, так і в насичених повітрям розчинах, що відрізняє досліджені наночастинки від традиційних органічних фотоініціаторів. В результаті аналізу кінетичних параметрів фотополімеризації встановлено, що процес відбувається за радикально-ланцюговим механізмом, причому основним маршрутом обриву ланцюга є рекомбінація макрорадикалів. Кінетичні дані також вказують на можливість участі в обриві ланцюга наночастинок $\text{Cd}_x\text{Zn}_{1-x}\text{S}$ і оксиду графену.

Ключові слова: *сульфід кадмію, сульфід цинку, оксид заліза, оксид графену, нанокристали, фотокаталіз, фотополімеризація*

Нанокристаллы полупроводников и оксид графена – чувствительные к видимому свету фотоинициаторы полимеризации акриламида в воде

А.Л. Стройук, С.Я. Кучмий, Н.С. Андрияшина

Институт физической химии им. Л.В. Писаржевского Национальной академии наук Украины
пр. Науки, 31, Киев, 03039, Украина, stroyuk@inphyschem-nas.kiev.ua

Изучена фотополимеризация акриламида в водных растворах, индуцированная при действии видимого света ($\lambda > 400$ нм) на коллоидные частицы $Cd_xZn_{1-x}S$, Fe_2O_3 и оксида графена. В зависимости от природы фотоинициатора, первичные радикалы образуются при восстановлении мономера фотогенерируемыми электронами зоны проводимости (в случае $Cd_xZn_{1-x}S$), окислении мономера фотогенерируемыми дырками валентной зоны (Fe_2O_3) или же в результате взаимодействия между мономером и свободными радикалами, образующимися при фотолизе инициатора (оксид графена). Скорость фотополимеризации возрастает пропорционально абсолютному значению потенциала зоны проводимости наночастиц $Cd_xZn_{1-x}S$, который определяется их составом. Фотополимеризация акриламида, индуцируемая наночастицами Fe_2O_3 , проходит одинаково эффективно как в дегазированных, так и в насыщенных воздухом растворах, что отличает изученные наночастицы от традиционных органических фотоинициаторов. В результате анализа кинетических параметров фотополимеризации установлено, что процесс идет по радикально-цепному механизму, причем основным маршрутом обрыва растущих цепей является рекомбинация макрорадикалов. Кинетические данные также указывают на возможность участия в обрыве цепи наночастиц $Cd_xZn_{1-x}S$ и оксида графена.

Ключевые слова: сульфид кадмия, сульфид цинка, оксид железа, оксид графена, нанокристаллы, фотокатализ, фотополимеризация

REFERENCES

1. Scranton A.B., Bowman C.N., Peiffer R.W. (Eds.) Photopolymerization: fundamentals and applications, New York, ACS, 1997, 242 p.
2. Belfield K.D. (Ed.) Photoinitiated polymerization, ACS Symp. Ser. 847, 2003, 570 p.
3. Крюков А.И., Шерстюк В.П., Дилунг Й.Й. Фотоперенос электрона и его прикладные аспекты, Киев, Наукова думка, 1982, 240 с.
4. Kargin V.A. (Ed.) Polymer encyclopedia, Moscow, Sovetskaya Entziklopedia, 1972, 1224 p. (in Russian).
5. Liska R., Schwager F., Maier C. et al. Water-soluble photopolymers for rapid prototyping of cellular materials, J. Appl. Polymer Sci., 97 (2005) 2286.
6. Davidenko N., Garcia O., Satsre R. The efficiency of titanocene as photoinitiator in the polymerization of dental formulations, J. Biomater. Sci. Polymer Ed., 14 (2003) 733.
7. Hoffmann A.J., Mills G., Yee H., Hoffmann M.R. Q-sized cadmium sulfide: synthesis, characterization, and efficiency of photoinitiation of polymerization of several vinylic monomers, J. Phys. Chem., 96 (1992) 5546.
8. Hoffmann A.J., Yee H., Mills G., Hoffmann M.R. Photoinitiated polymerization of methyl methacrylate using Q-sized zinc oxide colloids, J. Phys. Chem., 96 (1992) 5540.
9. Damm C. An acrylate polymerization initiated by iron doped titanium dioxide, J. Photochem. Photobiol. A, 181 (2006) 297.
10. Dong C., Ni X. The photopolymerization and characterization of methyl methacrylate initiated by nanosized titanium dioxide, J. Macromol. Sci., A41 (2004) 547.
11. Stroyuk A.L., Granchak V.M., Kuchmiy S.Ya. Photopolymerization of butylmethacrylate in 2-propanol induced by quantum-sized CdS particles, Theoret. Experim. Chem., 37 (2001) 170.
12. Stroyuk A.L., Granchak V.M., Korzhak A.V., Kuchmiy S.Ya. Photoinitiation of butylmethacrylate polymerization by colloidal semiconductor nanoparticles, J. Photochem. Photobiol. A, 162 (2004) 339.

13. Stroyuk A.L., Granchak V.M., Kuchmiy S.Ya. Photopolymerization of buthylmethacrylate induced by nanometer particles of hydrated iron(III) oxide, *Theoret. Experim. Chem.*, 37 (2001) 347.
14. Ojah R., Dolui S.K. Photopolymerization of methyl methacrylate using dye-sensitized semiconductor based photocatalyst, *J. Photochem. Photobiol. A*, 172 (2005) 121.
15. Stroyuk A.L., Granchak V.M., Kuchmiy S.Ya. Photopolymerization of buthylmethacrylate in the presence of ZnO nanoparticles sensitized to the visible light by xanthene dyes, *Theoret. Experim. Chem.*, 38 (2002) 324.
16. Ojah R., Dolui S.K. Solar radiation-induced polymerization of methyl methacrylate in the presence of semiconductor-based photocatalyst, *Sol. Energy Mater. & Sol. Cells*, 90 (2006) 1615.
17. Park S., Ruoff R.S. Chemical methods for the production of graphenes, *Nature Nanotechnol.*, 4 (2009) 217.
18. Dreyer D.R., Park S., Bielawski C.W., Ruoff R.S. The chemistry of graphene oxide, *Chem. Soc. Rev.*, 39 (2010) 228.
19. Compton O.C., Nguyen S.T. Graphene oxide, highly reduced graphene oxide, and graphene: versatile building blocks for carbon-based materials, *Small*, 6 (2010) 711.
20. Luo B., Liu S., Zhi L. Chemical approaches toward graphene-based nanomaterials and their applications in energy-related areas, *Small*, 8 (2012) 630.
21. Matsumoto Y., Koinuma M., Ida S. *et al.* Photoreaction of graphene oxide nanosheets in water, *J. Phys. Chem. C*, 115 (2011) 19280.
22. Ding Y.H., Zhang P., Zhuo Q. *et al.* A Green approach to the synthesis of reduced graphene oxide nanosheets under UV irradiation, *Nanotechnology*, 22 (2011) 215601.
23. Smirnov V.A., Arbutov A.A., Shul'ga Yu.M. *et al.* Photoreduction of graphite oxide, *High En. Chem.*, 45 (2011) 57.
24. Plotnikov V.G., Smirnov V.A., Alfimov M.A., Shul'ga Y.M. The graphite oxide photoreduction mechanism, *High En. Chem.*, 45 (2011) 411.
25. Shul'ga Y.M., Martynenko V.M., Muradyan V.E. *et al.* Gaseous products of thermo- and photo-reduction of graphite oxide, *Chem. Phys. Lett.*, 498 (2010) 287.
26. Stroyuk A.L., Andryushina N.S., Shcherban' N.D. *et al.* Photochemical reduction of colloidal graphene oxide, *Theoret. Experim. Chem.*, 48 (2012) 1.
27. Jeong G.H., Kim S.H., Kim M. *et al.* Direct synthesis of noble metal/graphene nanocomposites from graphite in water: photosynthesis, *Chem. Commun.*, 47 (2011) 12236.
28. Moon G., Kim H., Shin Y., Choi W. Chemical-free growth of metal nanoparticles on graphene oxide sheets under visible light irradiation, *RSC Adv.*, 2 (2012) 2205.
29. An X., Yu J.C. Graphene-based photocatalytic composites, *RSC Adv.*, 1 (2011) 1426.
30. Akhavan O. Photocatalytic reduction of graphene oxides hybridized by ZnO nanoparticles in ethanol, *Carbon*, 49 (2011) 11.
31. Feng R., Zhou W., Guan G. *et al.* Surface decoration of graphene by grafting polymerization using graphene oxide as the initiator, *J. Mater. Chem.*, 22 (2012) 3982.
32. Raevskaya A.E., Stroyuk A.L., Kryukov A.I., Kuchmiy S.Y. Structural and optical characteristics of $Cd_xZn_{1-x}S$ nanoparticles stabilized in aqueous solutions of polymers, *Theoret. Experim. Chem.*, 42 (2006) 181.
33. Deb P., Biswas T., Sen D. *et al.* Characteristics of Fe_2O_3 nanoparticles prepared by heat treatment of a nonaqueous powder precipitate, *J. Nanoparticle Res.*, 4 (2002) 91.
34. Garcia C., Zhang Y., DiSalvo F., Wiesner U. Mesoporous aluminosilicate materials with superparamagnetic $\gamma-Fe_2O_3$ particles embedded in the walls, *Angew. Chem. Int. Ed.*, 42 (2003) 1526.
35. Casas L., Roig A., Molins E. *et al.* Iron oxide nanoparticles hosted in silica aerogels, *Appl. Phys.*, 74 (2002) 591.
36. Woo K., Lee H.J., Ahn J.-P., Park Y.S. Sol-gel mediated synthesis of Fe_2O_3 nanorods, *Adv. Mater.*, 15 (2003) 1761.
37. Fistul V.I. Introduction into the semiconductor physics, Moscow, Vysshaya Shkola, 1984, 352 p. (in Russian).
38. Hannay N.B. (Ed.) *Semiconductors*, London, Chapman & Hall, 1962, 767 p.
39. Feng W., Nansheng D. Photochemistry of hydrolytic iron(III) species and photoinduced degradation of organic compounds. A minireview, *Chemosphere*, 41 (2000) 1137.
40. Bjorksten U., Moser J., Grätzel M. Photoelectrochemical studies on nanocrystalline hematite films, *Chem. Mater.*, 6 (1994) 858.

41. Gori M., Grüniger H.-R., Calzaferri G. Photochemical properties of sintered iron oxide, *J. Appl. Electrochem.*, 10 (1980) 345.
42. Bamford C.H., Barb W.G., Jenkins A.D., Onyon P.F. (Ed.) The kinetics of vinyl polymerization by radical mechanisms, London, Butterworths Scientific Publications, 1958, 318 p.
43. George M.H., Ghosh A. Effect of oxygen on the radical polymerization of acrylamide in ethanol and water, *J. Polym. Sci. Polym. Chem. Ed.*, 16 (1978) 981.
44. Bagdasaryan H.S. Theory of radical polymerization, Moscow, Nauka, 1966, 240 p. (in Russian).
45. Goronovski I.T., Nazarenko Y.P., Nekryatch E.F. Handbook of chemistry, Kyiv, Naukova dumka, 1974, 768 p. (in Russian).
46. Roy A.M., De G.C. Immobilisation of CdS, ZnS and mixed ZnS–CdS on filter paper Effect of hydrogen production from alkaline Na₂S/Na₂S₂O₃ solution, *J. Photochem. Photobiol. A*, 157 (2003) 87.
47. Kobayashi K., Kitaguchi K., Tanaka H. et al. Photogeneration of hydrogen from water over an alumina-supported ZnS–CdS catalyst, *J. Chem. Soc., Faraday Trans.*, 1 83 (1987) 1395.
48. Henglein A. Catalysis of Photochemical Reactions by Colloidal Semiconductors, *Pure Appl. Chem.*, 56 (1984) 1215.
49. Kryukov A.I., Kuchmiy S.Y., Pokhodenko V.D. Energetics of electron processes in semiconductor photocatalytic systems, *Theoret. Experim. Chem.*, 36 (2000) 63.
50. Zeug N., Bücheler J., Kisch H. Catalytic formation of hydrogen and carbon-carbon bonds on illuminated zinc sulfide generated from zinc dithiolenes, *J. Am. Chem. Soc.*, 107 (1985) 1459.
51. Bavykin D.V., Savinov E.N., Parmon V.N. Studies on the kinetics of interfacial electron transfer sensitized by colloidal CdS, *J. Photochem. Photobiol. A*, 130 (2000) 57.
52. Matsumoto H., Uchida H., Matsunaga T., Tanaka K. et al. Photoinduced reduction of viologens on size-separated CdS nano-crystals, *J. Phys. Chem.*, 98 (1994) 11549.
53. Faust B.C., Hoffmann M.R., Bahnemann D.W. Photocatalytic oxidation of sulfur dioxide in aqueous suspensions of α -Fe₂O₃, *J. Phys. Chem.*, 93 (1989) 6371.
54. Baizer M.M., Lund H. (Eds.) Organic electrochemistry, New York, Marcel Dekker, 1988, 1166 p.
55. Grätzel M. (Ed.) Energy resources through photochemistry and catalysis, New York, Academic Press, 1983, 570 p.
56. Fujishima A., Rao T.N., Tryk D.A. Titanium dioxide photocatalysis, *J. Photochem. Photobiol. C*, 1 (2000) 1.
57. Diebold U. The surface science of titanium dioxide, *Surf. Sci. Reports*, 48 (2003) 53.
58. Zhang J.Z. Interfacial charge carriers dynamics of colloidal semiconductor nanoparticles, *J. Phys. Chem. B*, 104 (2000) 7239.
59. Terenin A.N. The photonics of dyes and related compounds, Leningrad, Nauka, 1967, 618 p. (in Russian).
60. Nosaka Y., Fox M.A. Effect of light intensity on the quantum yield of photoinduced electron transfer from colloidal cadmium sulfide to methylviologen, *J. Phys. Chem.*, 90 (1986) 6521.
61. Biernat M., Rokicki G. Inhibicj a tlenowa procesów fotopolimeryzacji i sposoby jej ograniczania, *Polimery (polish ed.)*, 50 (2005) 631.
62. Awokola M., Lenhard W., Löffler H. et al. UV crosslinking of acryloyl functional polymers in the presence of oxygen, *Progress in Polym. Coatings*, 44 (2002) 211.
63. Wang C., Jin Q., Wang Y. et al. A green route to prepare graphite–poly(acrylic acid) and –poly(acrylamide) hybrids under γ -ray irradiation, *Mater. Lett.*, 68 (2012) 280.
64. Zhang B., Zhang Y., Peng C. et al. Preparation of polymer decorated graphene oxide by γ -ray induced graft polymerization, *Nanoscale*, 4 (2012) 1742.

Received 28.10.2014, accepted 26.11.2014